The Polymer Brush Model of Neurofilament Projections: Effect of Protein Composition

ARTICLE *in* BIOPHYSICAL JOURNAL · FEBRUARY 2010

Impact Factor: 3.97 · DOI: 10.1016/j.bpj.2009.10.033 · Source: PubMed

2 AUTHORS:

Ekaterina Zhulina
Institute of Macromolecular Compounds of …
182 PUBLICATIONS **6,209** CITATIONS
SEE PROFILE

Frans A M Leermakers
Wageningen University
288 PUBLICATIONS **4,645** CITATIONS
SEE PROFILE

The Polymer Brush Model of Neurofilament Projections: Effect of Protein Composition

E. B. Zhulina[†] and F. A. M. Leermakers[‡*]
[†]Institute of Macromolecular Compounds of the Russian Academy of Sciences, St. Petersburg, Russia; and [‡]Laboratory of Physical Chemistry and Colloid Science, Wageningen University, Wageningen, The Netherlands

ABSTRACT Applying self-consistent field theory, we consider a coarse-grained model for the polymerlike projections of neurofilament (NF) proteins that form a brush structure around neurofilaments. We focus on effects of molecular composition, which is the relative occurrence of NF-H, NF-M, and NF-L proteins, on the organization of NF projection domains. We consider NF brushes with selectively truncated projections, and with a varied ratio L:H:M of constituent tails. Our conclusion is that the NF brush structure is remarkably tolerant with respect to the variation in M and H chains. Results compare favorably with experimental data on model animals, provided that due attention is paid on the level of phosphorylation of the *KSP* repeats.

INTRODUCTION

The developments in computer simulations and field theoretical calculations have stimulated attempts to explore the organization of biomacromolecular assemblies with a detailed chemical composition resolution. Recently, we have applied the self-consistent field model of Scheutjens and Fleer (1–3,5) to probe the structure of neuronal intermediate filaments, or in short, neurofilaments (NFs), which are major constituents of the cytoskeleton in neurites (6).

NFs are composed of three subunit proteins labeled according to their molecular weights, namely: NF-L (light); NF-M (medium); and NF-H (heavy) (7,8). Each protein in this triplet has a rigid domain of ~310 amino acid (aa) residues, a globular head domain at the N-terminus, and a projection domain (a nonstructured flexible tail) at the C-terminus (9). In human NFs the numbers of aa residues are $N_H = 607$, $N_M = 504$, and $N_L = 142$ for the NF-H, NF-M, and NF-L projection domains, respectively (Human Intermediate Filament Database, http://www.interfil.org), and a typical stoichiometric ratio of the L:M:H proteins is 7:3:2. (10) This ratio, however, varies in different species and depends on neuronal type and developmental stage (11–13). Recent studies (14) have demonstrated that protein α-internexin is a fourth neurofilament component in small-caliber mature axons, which adds even more variability in composition of neurofilaments.

The flexible unstructured projection domains (tails) of NF proteins emanate from the filament core at average distances of 2–3 nm between the tails. The frequent emanation of the tails from the NF backbone justifies the application of polymer brush concepts to describe the properties of NF projections (15–19). Within a coarse-grained molecular model that makes use of the Scheutjens and Fleer method (1–3, 5), one can account for the primary aa sequence in the projection and implement both repulsive and attractive (cross-bridging) forces between NF brushes. The latter are believed to insure the integrity of NF network in axons (20,21).

In our previous studies (1,2) we focused on individual human NFs with a fixed (wild-type) protein composition L:M:H = 7:3:2, and analyzed how the physical chemical conditions (pH and ionic strength) as well as the degree of phosphorylation of the *KSP* repeats in the H- and M-tails affect the structure of NF brush. We have demonstrated that an increase in the level of phosphorylation leads to a cooperative relocation of the terminal *KEP* domain in the H-tail from the NF backbone to the periphery of the polymer brush formed by the M- and L-tails. Based on this translocation transition, we speculated that the phosphorylation of the projection domains might increase the interneurofilament spacing and enhance the propensity of H-tails to cross-bridge (1,2). In a subsequent publication (3), we incorporated the cross-bridging between the H-tails in our model and analyzed how the attraction between terminal *KEP* domains and the phosphorylation of the *KSP* motifs in the M- and H-tails affect the stability of a parallel array of interacting NFs. We demonstrated that an increase in cross-bridge frequency decreases the most probable (median) NF-NF spacing. At the same time, if the energy gain per cross-bridge is independent of the level of phosphorylation of the *KSP* repeats, both the median distance and the frequency of cross-bridges between the H-tails increase upon the progressive phosphorylation of the *KSP* motifs. So far, the cross-bridging between the M-tails was not taken into account. Preliminary Scheutjens and Fleer (1–3,5) modeling demonstrated that when both H- and M-chains are involved in the cross-links, the cross-bridging between M-tails might cause reversion of the stabilizing role of the phosphorylation. A detailed study of this process will be presented elsewhere.

Submitted July 3, 2009, and accepted for publication October 21, 2009.

*Correspondence: frans.leermakers@wur.nl

Editor: Nathan Andrew Baker.

0006-3495/10/02/0462/8 $2.00

doi: 10.1016/j.bpj.2009.10.033

Within this article we explore, using the same theoretical machinery, how variations in the stoichiometric ratio of L-, M-, and H-proteins change the structure of the NF brush. We first consider an individual (isolated) neurofilament and compare the brush-structure of projection domains for the wild-type W-NF with those of filaments with truncated (deleted) tails (M, H, or L), and of filaments with progressively substituted M- with H-tails. The analysis of these systems allows us to better identify the roles of the individual tails and to establish the hierarchy of interactions within the NF brush. We demonstrate that the M-H interactions are weaker than the interactions of the M-L and H-L. However, the NF thickness and compressibility are nonetheless governed by the long tails that reside outside. We then compare the predictions of Scheutjens and Fleer (1–3,5) model with the experimental data from the literature.

MODEL

The application of the Scheutjens and Fleer (1–3,5) approach to NF brushes requires two levels of coarse-graining. First, each of the aa residues in a NF projection domain is modeled as an isotropic monomer with size $a = 0.6$ nm. Second, the aa residues in the NF tails are divided into five groups (C, M, P, N, and A). In short, the basic and the acidic aa residues are assigned to groups P and M, respectively, whereas the serines subject to phosphorylation are marked C. All the other aa residues with moderate and poor solubility are placed in respective *N* and A groups. The solution salinity is varied by additions of small ions, such as, e.g., Na and Cl. The coarse-grained sequences of H-, M-, and L-projections were presented in Zhulina and Leermakers (1). The set of various interaction parameters used for each of the group (C, M, P, N, and A) and other details of the Scheutjens and Fleer (1–3,5) method were summarized in Leermakers and Zhulina (3) . The Flory-Huggins interaction parameters are zero except for $\chi_{ANa} = \chi_{ACl} = \chi_{AW} = 2$, $\chi_{AP} = \chi_{AN} = \chi_{AM} = \chi_{AC} = 1$ and $\chi_{WN} = \chi_{WC} = 0.6$.

The degree of enzymatic phosphorylation of NF-M and NF-H projection domains is implemented by assigning a valence $-2 \le \nu_C \le 0$ to the serines present in the *KSP* repeats. Here $\nu_C = 0$ is the dephosphorylated state. A value of $\nu_C = -1$ corresponds to half of the *KSP* repeats being phosphorylated and when all *KSP* repeats are decorated by phosphates, $\nu_C = -2$. All other serines and threonines are assumed to be unaffected by the phosphorylation.

The coarse-grained projections are tethered to a solid cylinder with radius $R = 8a = 5$ nm, which mimics the NF core. For all NF brushes considered in this article, exactly 12 projections are tethered per core segment with length $l = 25a = 15$ nm. Such grafting density corresponds to 32 projections per length of coiled-coil domain $l_c = 40$ nm. In a wild-type W-NF with molar ratio L:M:H = 7:3:2, one therefore finds 7 L-, 3 M-, and 2 H-tails and distances $d_L = l/7$, $d_M = l/3$, and $d_H = l/2$ between projections L, M, and H, respectively, along the backbone. The distance d_i specifies the dimensionless coverage $\Theta_i = N_i a/d_i$ (where N_i is number of monomers in the projection of type i = L, M, H), which amounts to $\Theta_L^W = 39.76$, $\Theta_M^W = 60.48$, and $\Theta_H^W = 48.56$ in a wild-type, W-NF. In the following, we use values of Θ_i (i = L, M, H) to specify the NF composition. For example, in a pure L-filament all 12 projections are L-tails and $\Theta_H = 0$, $\Theta_M = 0$, and $\Theta_L = 12 \times 142/25 = 68.16$. In NFs for which tails of type i are truncated, we implemented $\Theta_i = 0$, whereas for all others, $\Theta_{k \neq i}$ are kept unchanged (as in wild-type).

For models of NFs that form in the axoplasm of animals with some altered NF protein ratio (mutants), we estimated Θ_i as follows. We assume that for a given mutant the NF still comprises 32 protein molecules per cross section, and we further assume that the distribution of all its components is uniform over the neurofilaments within an axon. In a wild-type NF with a molar ratio L:M:H = 7:3:2, the total number Ω_i^W of protein molecules of type i per length l of axon specifies the corresponding number P^W of filaments in the axonal cross section as

$$P^W = \frac{\left(\Omega_L^W + \Omega_M^W + \Omega_H^W\right)}{12} = \frac{\Omega_L^W}{7} = \frac{\Omega_M^W}{3} = \frac{\Omega_H^W}{2}. \quad (1)$$

In mutants with $\Omega_i \neq \Omega_i^W$, the total number of filaments in an axonal cross section is $P = (\Omega_L + \Omega_M + \Omega_H)/12$, and

$$\frac{P}{P^W} = \frac{7}{12}\left(\frac{\Omega_L}{\Omega_L^W}\right) + \frac{3}{12}\left(\frac{\Omega_M}{\Omega_M^W}\right) + \frac{2}{12}\left(\frac{\Omega_H}{\Omega_H^W}\right). \quad (2)$$

Correspondingly, the coverage

$$\Theta_i = \Theta_i^W \frac{\Omega_i}{\Omega_i^W}\frac{P^W}{P}. \quad (3)$$

Hence, the experimentally measurable ratios Ω_i/Ω_i^W (i = L, M, and H) specify the values of Θ_i for a particular mutant through Eqs. 2 and 3.

As before (1,2), we use the one-gradient version of the Scheutjens and Fleer (1–3,5) model. That is, their model accounts for concentration gradients of all the components in the direction normal to the neurofilament core, whereas in lateral and angular directions the densities are averaged. The system (cell) size is limited in the radial r-direction, such that $0 \le r \le D$. At the outer edge of the system $r = D$ we impose reflecting boundary condition. Effectively, enclosing a central NF in a volume with mirror boundary conditions (shown in Fig. 1 by the *central dashed circle*) implies that we consider a network of parallel NFs. Due to the relatively low concentration of aa residues at the periphery of these NF brushes, a certain interpenetration of filaments is allowed (as depicted in Fig. 1), and the NF-NF distance H is related to cell size ($R + D$) as $H = \sqrt{3}(D + R)$. For a chosen set of simulation parameters, any variation in H due to changes in the NF composition

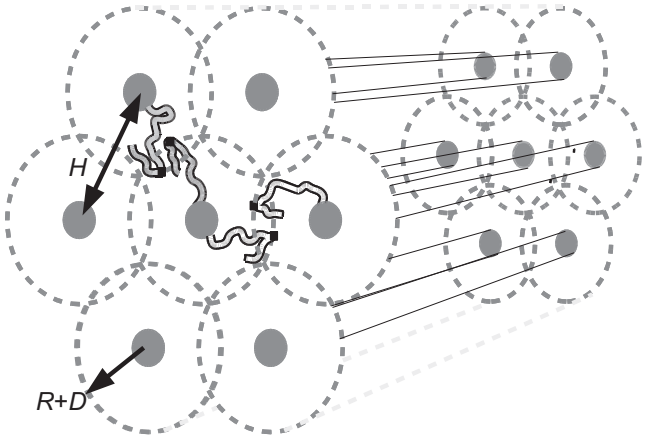

FIGURE 1 Schematic illustration of the NF network, here consisting of seven NFs. In the front cross section, the shaded spheres (with radius R) are the cores of the neurofilaments from which the L- (not shown), M- (interior of line is *shaded*), and H- (interior of line is *open*) projections come out. The solid squares (placed at the *dashed circle* of radius $R + D$ that represents the boundary of the simulation box) indicate the constrained (pinched) aa residues to simulate the effect of cross-bridging between M- and H- chains. The NF-NF distance is H. The parallel alignment of the NF is illustrated by presenting a cross section at some distance from the front cross section. The thin lines are used to guide the eye and to show how the cores run parallel.

gives information on how different projections interact in a NF brush.

To compare the predictions of the Scheutjens and Fleer (1–3,5) model with experiments, we imposed cross-bridging between M- and H-tails. We consider here the cases of 0% and 100% cross-bridging between the long tails and report the corresponding NF-NF distances as $H_{0\%}$ and $H_{100\%}$, in these two limits. (The distances $H_{0\%}$ and $H_{100\%}$ serve as respective upper and lower boundaries for the NF-NF spacing with arbitrary degrees of M-M and H-H cross-bridging.) We assume that an H-H cross-bridge incorporates the whole *KEP* domain (of 191 aa residues) (20). Although an M-M cross-bridge might involve a different number of aa residues (21), in this article we assume that the cross-bridging domains for M- and H-tails are close in length and hence we have chosen the terminal 200 aa residues of the M-tail as the M-M cross-bridging domain.

At 0% cross-bridging, the positions of aa residues in the M- and H-tails are unrestricted, and the terminal domains can be found anywhere inside the brush volume. The 100% M-M and H-H cross-bridging is modeled as follows:

1. In a cross-bridge, the binding domain (*KEP* domain for H-tail and terminal 200 aa residues for M-tail) is assumed to overlap with a similar domain from an adjacent NF to form a symmetric complex comprising both domains.
2. The central aa residues of the two binding domains are localized (pinned) at the external boundary of the system volume, i.e., at a distance $r = D$ from the core. This pinned segment is shown in Fig. 1 by a solid square. Due to the imposed mirror boundary condition, the remaining fragment of each binding domain is reflected inside the NF volume and mimics a similar fragment of a binding domain from the neighboring NF.

The Scheutjens and Fleer (1–3,5) model allows for the direct evaluation of the free energy $F^{\text{int}}(D)$ (per unit length a of the backbone) for the system with both unrestricted and restricted positions of specified monomers. We can therefore evaluate $F^{\text{int}}_{0\%}(D)$ and $F^{\text{int}}_{100\%}(D)$, where subscripts indicate the percentage of cross-bridges between the long tails. In this article, we mostly focus on the pH and the salt concentrations close to intracellular physiological values (pH = 7 and $c_s = 0.15$ M of 1:1 salt, referred to below as physiological conditions).

RESULTS AND DISCUSSION

To characterize the structure of an individual NF brush with altered L:M:H ratio, we considered the polymer density distributions $\phi_i(r)$ of individual tails (i = L, M, H) in Fig. 2. Such distributions were discussed in detail for a wild-type NF in the literature (1,2) and are repeated here for comparison. To obtain $\phi_i(r)$, we placed an NF in a cylindrical tube of large diameter D and imposed 0%

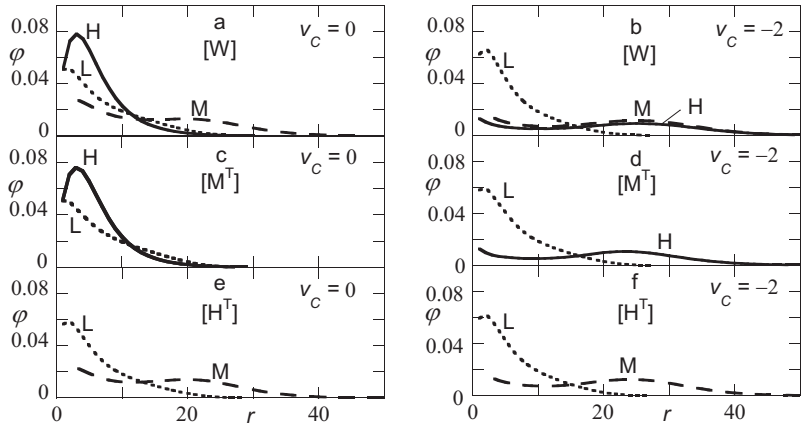

FIGURE 2 Radial volume fraction profiles $\phi(r)$ of the L- (*dotted*), M- (*dashed*), and H-chains (*solid*) at pH = 7, $c_s = 0.15$ M. (*a*) Wild-type $v_C = 0$; (*b*) wild-type $v_C = -2$; (*c*) truncated M-chains (L and H only) $v_C = 0$; (*d*) truncated M-chains $v_C = -2$; (*e*) truncated H-chains (L and M only) $v_C = 0$; and (*f*) truncated H-chains $v_C = -2$.

cross-bridging between the long projections. The left panels (Fig. 2, *a*, *c*, and *e*) correspond to the absence of phosphorylation of the *KSP* repeats. The right panels (Fig. 2, *b*, *d*, and *f*) are for the full phosphorylation of the *KSP* repeats. In Fig. 2, *c* and *d*, the selective truncation of M-tails is given (labeled as M^T-NF), whereas in Fig. 2, *e* and *f*, the results for the truncation of the H-tails (H^T-NF) are shown.

Typically, the H-chain responds strongly to a change of the degree of phosphorylation, irrespective of whether the M-chains are present (wild-type) or not (M^T). The H chains evolve from a loop configuration at $\nu_C = 0$ into a flower configuration at $\nu_C = -2$. For the other chains the volume fraction profiles of the remaining projections appear rather insensitive for any phosphorylation level of the *KSP* motifs. Therefore, the truncation of either the M- or H-chain has no big effect on how the remaining chains respond to the phosphorylation of the *KSP* repeats.

The truncation of the shortest L-tails, however, leads to a noticeable change in the volume fraction profiles of both M- and H-tails (F. A. M. Leermakers and E. B. Zhulina, unpublished). In a dephosphorylated state of such filament (labeled as L^T-NF), the M-tail becomes less extended and loses its flowerlike configuration (1), whereas the H-tail becomes less confined near the NF core. In a fully phosphorylated state, both M- and H-tails demonstrate a distribution that is characteristic for a cylindrical polyelectrolyte brush (with no flowerlike conformations). These results confirm that in the framework of the Scheutjens and Fleer (1–3,5) model, the L-tails play an important mediating role in the organization of an individual NF. The short brush of negatively charged L-tails (with no *KSP* motifs) creates a potential-well near the NF core that can regulate the conformations of the longer projections in a phosphorylation-dependent manner. These effects are discussed elsewhere (F. A. M. Leermakers and E. B. Zhulina, unpublished).

Due to different charge distributions within the long projections, the relative strength of the M-L and of the H-L interactions differ. Note that in wild-type NFs with molar ratio M:H = 3:2 one finds that for every seven L-tails, there are, in total, five long projections (3 M projections and 2 H projections). To probe the relative strength of the M-L and the H-L interactions we considered a set of NFs (labeled as M0, M1, M2, M3, M4, and M5, according to the number $0 \le n_M \le 5$ of M-tails) at a fixed value of $\Theta_L = 39.76$.

To quantitatively characterize the thickness of NF brush with altered protein composition, we placed the NF in a cylindrical tube of radius $R + D$ and examined the behavior of the system free energy $F^{int}(D)$ as a function of D.

In the current parameter setting, NFs with long projections demonstrate a nonmonotonic dependence of the free energy $F^{int}(D)$ upon a compression (that is, a decrease in D). Fig. 3 shows how $F^{int}(D)$ depends on D at the frequency of cross-bridges 0% for a NF brush wherein all M-tails are substituted by H-tails (M0-NF), at three different levels of phosphorylation (indicated at the *curves*). Note that the value of free

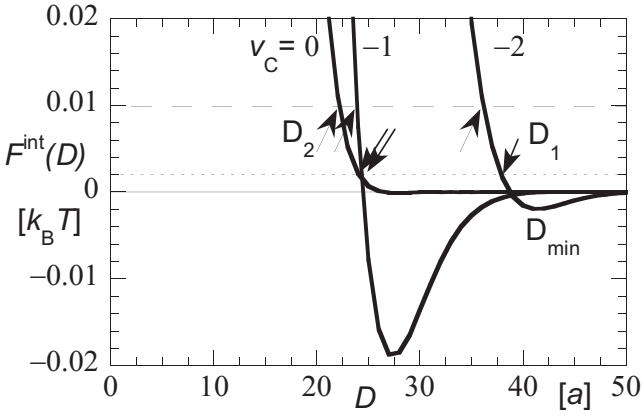

FIGURE 3 Free energy $F^{int}(D)$ in units of k_BT with D in units of a for M0-NF at physiological conditions. The arrows pointing downward indicate values of D_1 (corresponding to $F^{int} = 0.002\ k_BT$ marked by the *horizontal dotted line*). Arrows pointing upward mark D_2 (corresponding to $F^{int} = 0.01\ k_BT$ marked by the *horizontal dashed line*). The minimum of the interaction curves is denoted by D_{min}. The degree of phosphorylation of the *KSP* repeats is indicated. Zero percent is phosphorylated for $\nu_C = 0$, 50% is phosphorylated for $\nu_C = -1$, and 100% is phosphorylated for $\nu_C = -2$.

energy at $D \to \infty$ is subtracted to highlight the behavior of the free energy at small compressions. An initial decrease in D leads to the appearance of a minimum, which indicates weak nonspecific attraction between neighboring NFs. The depth of this minimum F^{int}_{min} rapidly increases upon a decrease in the ionic strength in the solution, pointing at a possible role of the nonelectrostatic tail-tail interactions (3). When $F^{int}_{min} \le 0.002\ k_BT$, the energy of attraction per persistence length $l_p \simeq 480$ nm is $\le 1\ k_BT$, and thermal fluctuations destroy the attraction-driven associations between the filaments. When, however, $F^{int}_{min} > 0.002\ k_BT$, the attraction between filaments might establish an optimal NF-NF distance, at $H_{min} = \sqrt{3}(R + D_{min})$, where D_{min} is the position of the minimum on the $F^{int}(D)$ curve. A further decrease in D results in a free energy increase, indicating a repulsion between the NF brushes. The onset of repulsion can be specified as $F^{int}(D) \simeq 0.002\ k_BT$, indicated by the dotted line in Fig. 3. This value corresponds to the energy of repulsion per NF persistence length $l_p \simeq 480$ nm of $\simeq 1\ k_BT$, and is reached at $D = D_1$. The increase in $F^{int}(D)$ up to $0.01\ k_BT$ (indicated by the *horizontal dashed line*) gives the value of compression D_2 when the free energy of repulsion amounts to $\simeq 10\ k_BT$ per persistence length l_p (*up-arrows*). Such repulsion is clearly sufficient to withstand the thermal fluctuations and keep the NFs apart. We use all three parameters—D_{min}, D_1, and D_2—as indicators of the NF brush thickness and collect them for NFs with truncated projections in Table 1 and for NFs with altered H:M ratio in Table 2.

As is extracted from Table 1, the three parameters, D_{min}, D_1, and D_2, provide rather close estimates for the NF brush thickness. The maximal difference $D_{min} - D_2$ is ~4 nm, whereas $D_1 - D_2 \simeq 1$ nm. In terms of the NF brush thickness, cutting off the H-tails is less significant than removing

TABLE 1 Comparison of knock-out data and model results for the NF brush thickness

				$v_C = 0$			$v_C = -1$			$v_C = -2$		
	Θ_L	Θ_M	Θ_H	D_{min}	D_1	D_2	D_{min}	D_1	D_2	D_{min}	D_1	D_2
W	39.76	60.48	48.56	21	18	17	22	19	18	26	23	22
H^T	39.76	60.48	0	20	18	17	23	20	19	27	22	20
M^T	39.76	0	48.56	17	14	13	17	14	14	23	20	19
L^T	0	60.48	48.56	13	11	10	18	16	14	23	20	19
M^TH^T	39.76	0	0	—	14	13	—	14	13	—	14	13

Thickness in nm of an NF brush determined by 1), the position of the minimum (D_{min}); and 2), the mechanical thickness obtained from an increase in $F^{int} = +0.002\ k_BT$ (D_1) and $+0.01\ k_BT$ (D_2). Underlined numbers correspond to values with a $\leq 0.002\ k_BT$.

the M-tails, particularly at low ($v_C = 0$) and intermediate ($v_C = -1$) levels of phosphorylation of *KSP* motifs. Whereas the thickness of H^T-NFs is almost unchanged compared to W-NFs, the thickness of M^T-NFs drops by ~20–25% at $v_C = 0$ and $v_C = -1$, and remains lower by ~10% in a fully phosphorylated state $v_C = -2$. The elimination of both M- and H-tails leads to a more dramatic decrease in the NF brush thickness. Due to the lack of *KSP* motifs in the L-tails, the thickness of H^TM^T-NFs becomes independent of the phosphorylation and decreases by $\simeq 40\%$ with respect to fully phosphorylated W-NFs. The values of $D_1 = 14$ nm and $D_2 = 13$ nm for H^TM^T-NF are close to experimentally measured thickness of L-brush ($\simeq 14$ nm) in reconstituted filaments of NF-L proteins in the solution (22). Finally, deleting the L-tails leads to an even stronger decrease in the NF brush thickness at $v_C = 0$, but full phosphorylation of the *KSP* motifs makes the thickness of L^T-NFs equal to that of M^T-NFs and closer to that of W-NFs (F. A. M. Leermakers and E. B. Zhulina, unpublished).

The data of Table 2 indicate that the substitution of H-tails by M-tails leads to a gradual increase in thickness of the NF brush. The effect is most pronounced at low and intermediate levels of phosphorylation ($v_C = 0$ and $v_C = -1$). At $v_C = 0$, a full substitution of H-tails by M-tails (i.e., a transition from M0-NF to M5-NF) leads to an increase in thickness of the NF brush by ~25%. However, at full phosphorylation of the *KSP* motifs ($v_C = -2$), a mild increase in the NF brush thickness is detected only for the M5-NF. A weak dependence of the NF brush thickness on the M:H ratio at $v_C = -2$ is explained by noting that when all *KSP* motifs are phosphorylated, the H- and M-chains are almost equally charged.

We now turn to in vivo data obtained for NF-M and NF-H knockout mice (23,24), and transgenic mice with selectively truncated NF projections (25,26) and altered NF subunit composition (27). The morphological analysis of neurons in M-null mutation mice (23) indicated that the distributions of nearest-neighbor NF-NF distances in axons of NF-M deficient animals were only slightly shifted, and no difference in median (most frequent) NF-NF spacing was detected (47 nm in both wild-type and M-null mutation species). In mutants lacking the NF-H subunit, the median NF-NF distance also stayed intact (47 nm) (24).

In more recent studies (25,26), the long projections were selectively modified. The replacement of the NF gene by one deleted in this NF tail led to no change in the ratio of NF subunits in transgenic mice and this made it possible to examine the axoplasm with selectively deleted NF-tails. When the H-tails were deleted (25), the distribution of nearest-neighbor distances was almost unaffected compared to wild-type animals, although a slight modification of the maximum (shift in median distance from ≈ 50 nm to ≈ 45 nm) is detectable in Fig. 4 of Rao et al. (25). Deleting all M-tails led to more severe effects (26). Now the distribution of nearest-neighbor distances shifted noticeably, and the median NF-NF spacing decreased from 45 nm to 39 nm. However, the filaments remained aligned longitudinally (presumably due to cross-bridges between the H-tails). Deletion of both M- and H-tails decreased the median spacing to 30 nm, eliminated almost all cross-bridges

TABLE 2 Comparison of mutant data and model results for the NF brush thickness

				$v_C = 0$			$v_C = -1$			$v_C = -2$		
	Θ_L	Θ_M	Θ_H	D_{min}	D_1	D_2	D_{min}	D_1	D_2	D_{min}	D_1	D_2
M0	39.76	0	121.40	17	14	13	17	15	14	25	23	22
M1	39.76	20.16	97.12	18	17	15	18	16	16	25	23	22
M2	39.76	40.32	72.84	21	17	16	20	18	17	25	23	22
M3	39.76	60.48	48.56	21	18	17	22	19	18	26	23	22
M4	39.76	80.64	24.28	20	18	17	23	20	19	26	23	22
M5	39.76	100.80	0	20	18	17	23	21	20	28	25	22

Thickness in nm of an NF brush determined by 1), the position of the minimum (D_{min}); and 2), the mechanical thickness obtained from an increase in $F^{int} = +0.002\ k_BT$ (D_1) and $+0.01\ k_BT$ (D_2). Underlined numbers correspond to values with a minimum $\leq 0.002\ k_BT$.

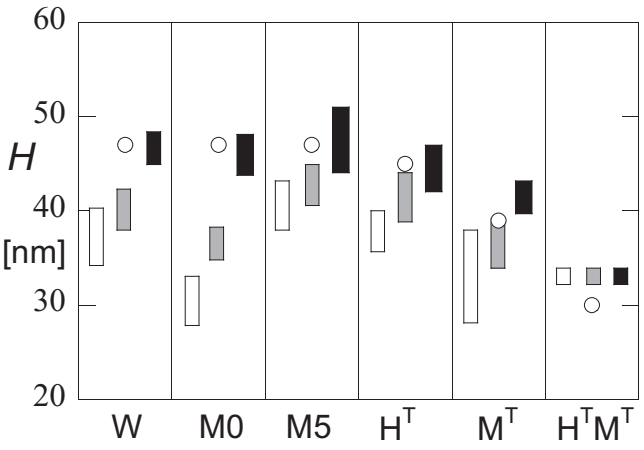

FIGURE 4 The median distance H in nm for model animals with knockout NF proteins and NF proteins with truncated tails (23–26). Experimental data are given by the circles, the Scheutjens and Fleer (1–3,5) model predictions are shown by rectangles. The upper and lower limits of the rectangles represent the $H_{0\%}$ and $H_{100\%}$, respectively. Solid rectangles correspond to the degree of phosphorylation. Open rectangles correspond to $v_C = 0$, the shaded ones to $v_C = -1$, and the solid rectangles are for $v_C = -2$.

between filaments, and this reduced the organization of the axoplasm (26).

To compare in vivo data with the results of the Scheutjens and Fleer (1–3,5) model, we presumed that the NF compositions in NF-M and NF-H knockout mice correspond to those in M0 (all M-tails are substituted by H-tails) and M5 (all H-tails are substituted by M-tails) filaments, respectively. Similarly, the NF projections in transgenic mice with deleted H-, M-, and both, H- and M-tails are modeled as respective H^T-, M^T- and H^TM^T-NF brushes. Because cross-bridge frequencies in model animals are unknown, the two limiting cases for the cross-bridging between the long tails—namely 0% and 100%—were considered. As discussed in our previous publication (3), the pinning of the terminal domains of long projections in cross-bridges gives rise to a well-defined minimum in the free energy curve $F^{int}(D)$. Such behavior was found for all NF brushes with long tails, and the values of D_{min} were used to calculate the median NF-NF distance $H_{100\%} = \sqrt{3}(R + D_{min})$ for all the mutants.

In Fig. 4 we have collected the median NF-NF distances in axons of a wild-type animal, M-null and H-null mutants (23,24), mice with deleted H-tails (25), deleted M-tails (26), and deleted both H- and M-tails (26). These data are shown by the open circles. In the same graph we have plotted the theoretical predictions. For these we used rectangles. The solid rectangle indicates the level of phosphorylation assumed in the calculations (that is, *open* for $v_C = 0$, *shaded* for $v_C = -1$, and *solid* for $v_C = -2$). The upper boundary of each rectangle corresponds to 0% cross-bridging between filaments. Here, $H_{0\%}$ was calculated as $H_{0\%} = \sqrt{3}(R + D)$, where $D = D_{min}$ if depth of the minimum $F^{int}_{min} \geq 0.002\ k_BT$, and $D = D_1$ otherwise. The values of D_{min} and D_1 for the W-, M0-, M5-, H^T-, M^T- and H^TM^T-NFs were taken from Tables 1 and 2. The lower boundary of each rectangle corresponds to 100% cross-bridging between the remaining long projections, $H_{100\%}$. As proven by the correlation between the predictions and the experimental data, the Scheutjens and Fleer (1–3,5) model reproduces the experimentally observed trend. Even better, the calculations give close-to in vivo values for the median NF-NF spacing when the tails are heavily phosphorylated ($v_C = -2$, *solid rectangles*).

We now focus on in vivo data for mutants with an altered ratio of NF subunits (27). Six lines of transgenic mice (labeled as L, M, H, LM, LH, and MH according to type(s) of elevated proteins) were investigated, and the subunit levels were quantified in each of the mutants (Table 1 in (27)). Under the assumption that the proteins are distributed uniformly among all filaments, the L:M:H ratio in an individual NF coincides with the average subunit ratio in these neuronal cells. In this approximation the NF protein ratios in the axoplasms determine the values of Ω_i/Ω_i^W (i = L, M, and H) for an individual NF. For example, in mutant L, the concentration levels of NF-L, NF-M, and NF-H proteins were elevated by 230%, 115%, and 110% with respect to a wild-type animal (27). Hence, the assumption of uniform protein distribution gives Ω_i/Ω_i^W as $\Omega_L/\Omega_L^W = 2.30$, $\Omega_M/\Omega_M^W = 1.15$, and $\Omega_H/\Omega_H^W = 1.10$. The morphological analysis of the axoplasm in spinal motor neurons produced the average NF-NF spacing H_{av}. In the corresponding theoretical analysis of the median NF-NF distances, we computed the Θ_i coverages of tails i = L, M, and H for each of the mutants according to Eqs. 2 and 3, and then determined $H_{0\%}$ and $H_{100\%}$ (as explained above). In Fig. 5 we have collected the average experimental NF-NF spacings H_{av}. The data points were extracted from Fig. 8 in Xu et al. (27) and shown by circles with error bars. The

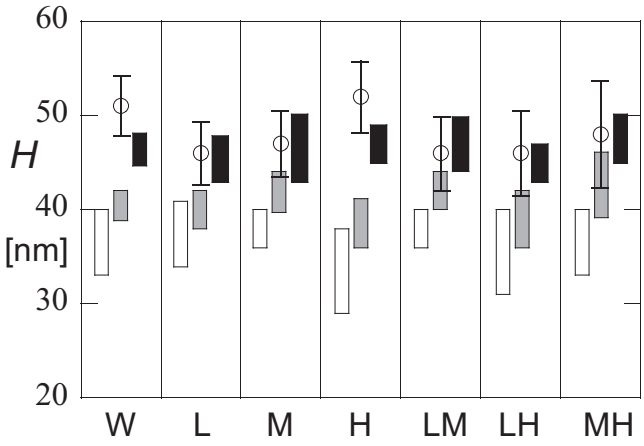

FIGURE 5 The average distance H_{av} in nm for model animals with varied NF protein ratio (27) and theoretical median distance H. Experimental data are given by the circles with error bars, the Scheutjens and Fleer (1–3,5) model predictions are shown by rectangles (see legend to Fig. 4).

corresponding theoretical median NF-NF distances H are again shown by rectangles. As explained for Fig. 4, the upper and lower boundaries of each rectangle corresponds to $H_{0\%}$ and $H_{100\%}$ values, respectively, whereas the solid rectangle indicates the level of phosphorylation of the *KSP* motifs. The solid rectangles ($v_C = -2$) fit the experimental data better, which is consistent with the expected high levels of phosphorylation of the *KSP* motifs in these axons. Note that for a given parameter set, the comparison between the theoretical model and the experiment data is direct and requires no adjustable parameters.

CONCLUSIONS

In this article we applied the one-gradient version of the Scheutjens and Fleer (1–3,5) model to explore the equilibrium structure of a neurofilament with altered H:M:L tail ratio. The projection domains of NF-L, NF-M, and NF-H proteins were coarse-grained to conserve the major features of the actual primary sequence of aa residues. We have introduced five groups of monomers (A, N, P, M, and C) that collect the aa residues with different charges and hydrophobicities, and imposed a cylindrical symmetry on the NFs. This is justified by the large aspect ratio $l_p/D >> 1$ of these filaments. The presence of neighboring neurofilaments was accounted for by placing a given neurofilament in a cylindrical tube of radius $R + D$ with reflecting (mirror) boundary. Such Ansatz allowed us to study the structure of individual NFs (at large D) and to examine the effects of cross-bridging of parallel oriented NFs.

The truncation (removal) of intermediate M-tails affects the NF brush structure more than deleting the longest H-tails. Whereas the thickness of such H^T-NF is almost unchanged compared to wild-type W-NF, the thickness of M^T-NF drops by ~20–25% at $v_C = 0$ and $v_C = -1$, and remains lower by ~10% in a fully phosphorylated state $v_C = -2$. Cutting away both M- and H-tails leads to a more dramatic decrease in the NF brush thickness. This thickness becomes independent of the degree of phosphorylation of the *KSP* motifs and decreases by $\simeq 40\%$ with respect to fully phosphorylated W-NF. Finally, a truncation of the L-tails (F. A. M. Leermakers and E. B. Zhulina, unpublished) leads to even stronger decrease in the NF brush thickness at $v_C = 0$, but full phosphorylation of the *KSP* motifs makes the thickness of L^T-NF equal to that of M^T-NF and closer to that of W-NF.

Progressively exchanging M- by H-tails revealed different affinities of the tail-tail interactions. Although the NF brush thickness demonstrated modest variations upon the substitution of the H-tails by M-tails, the free energy of NF-NF interaction showed a more peculiar behavior. A noticeable minimum in the curve for $F^{int}(D)$ for NFs enriched in H-tails is found, suggesting some nonspecific hydrophobic attraction between filaments, particularly at intermediate levels of phosphorylation of *KSP* motifs.

The authors acknowledge financial support from the Dutch National Science Foundation and the Russian Foundation for Basic Research through joint project No. 047-017-026 (''Polymers in Nanomedicine: Design, Synthesis and Study of Inter-Polymer and Polymer-Virus Complexes in Search of Novel Pharmaceutical Strategies''). E.B.Z. acknowledges partial support from the Russian Foundation for Basic Research (RFBR grant No. 08-03-00336).

REFERENCES

1. Zhulina, E. B., and F. A. M. Leermakers. 2007. A self-consistent field analysis of the neurofilament brush with amino-acid resolution. *Biophys. J.* 93:1421–1430.
2. Zhulina, E. B., and F. A. M. Leermakers. 2007. Effect of the ionic strength and pH on the equilibrium structure of a neurofilament brush. *Biophys. J.* 93:1452–1463.
3. Leermakers, F. A. M., and E. B. Zhulina. 2008. Self-consistent field modeling of the neurofilament network. *Biophys. Rev. Lett.* 3:459–489.
4. Reference deleted in proof.
5. Zhulina, E. B., and F. A. M. Leermakers. 2009. On the polyelectrolyte brush model of neurofilaments. *Soft Matter*. 42:5360–5371.
6. Fuchs, E., and D. W. Cleveland. 1998. A structural scaffolding of intermediate filaments in health and disease. *Science*. 279:514–519.
7. Hoffman, P. N., and R. J. Lasek. 1975. The slow component of axonal transport. Identification of major structural polypeptides of the axon and their generality among mammalian neurons. *J. Cell Biol.* 66:351–366.
8. Liem, R. K. H., S.-H. Yen, …, M. J. Shelanski. 1978. Intermediate filaments in nervous system. *J. Cell Biol.* 79:537–645.
9. Herrmann, H., and U. Aebi. 2004. Intermediate filaments: molecular structure, assembly mechanism, and integration into functionally distinct intracellular scaffolds. *Annu. Rev. Biochem.* 73:749–789.
10. Janmey, P. A., J.-F. Leterrier, and H. Herrmann. 2003. Assembly and structure of neurofilaments. *Curr. Opin. Coll. Interface Sci.* 8:40–47.
11. Shaw, G., and K. Weber. 1982. Differential expression of neurofilament triplet proteins in brain development. *Nature*. 298:277–279.
12. Drake, P. F., and R. J. Lasek. 1984. Regional differences in the neuronal cytoskeleton. *J. Neurosci.* 4:1173–1186.
13. Tsuda, M., T. Tashiro, and Y. Komiya. 2000. Selective solubilization of high-molecular-mass neurofilament subunit during nerve regeneration. *J. Neurochem.* 74:860–868.
14. Yuan, A., M. V. Rao, …, R. A. Nixon. 2006. Alpha-internexin is structurally and functionally associated with the neurofilament triplet proteins in the mature CNS. *J. Neurosci.* 26:10006–10019.
15. Brown, H. G., and J. H. Hoh. 1997. Entropic exclusion by neurofilament sidearms: a mechanism for maintaining interfilament spacing. *Biochemistry*. 36:15035–15040.
16. Mukhopadhyay, R., S. Kumar, and J. H. Hoh. 2004. Molecular mechanisms for organizing the neuronal cytoskeleton. *Bioessays*. 26:1–9.
17. Hoh, J. H. 1998. Functional protein domains from the thermally driven motion of polypeptide chains: a proposal. *Proteins Struct. Funct. Genet.* 32:223–228.
18. Kumar, S., X. Yin, …, M. E. Paulaitis. 2002. Relating interactions between neurofilaments to the structure of axonal neurofilament distributions through polymer brush models. *Biophys. J.* 82:2360–2372.
19. Lele, T. P., and S. Kumar. 2007. Brushes, cables, and anchors: recent insights into multiscale assembly and mechanics of cellular structural networks. *Cell Biochem. Biophys.* 47:348–360.
20. Chen, J., T. Nakata, …, N. Hirokawa. 2000. The C-terminal tail domain of neurofilament protein-H (NF-H) forms the crossbridges and regulates neurofilament bundle formation. *J. Cell Sci.* 113:3861–3869.
21. Nakagawa, T., J. Chen, …, N. Hirokawa. 1995. Two distinct functions of the carboxyl-terminal tail domain of NF-M upon neurofilament assembly: cross-bridge formation and longitudinal elongation of filaments. *J. Cell Biol.* 129:411–429.

22. Jones, J. B., and C. R. Safinya. 2008. Interplay between liquid crystalline and isotropic gels in self-assembled neurofilament networks. *Biophys. J.* 95:723–835.

23. Elder, G. A., V. L. Friedrich, Jr., …, R. A. Lazzarini. 1998. Absence of the mid-sized neurofilament subunit decreases axonal calibers, levels of light neurofilament (NF-L), and neurofilament content. *J. Cell Biol.* 141:727–739.

24. Elder, G. A., V. L. Friedrich, Jr., …, R. A. Lazzarini. 1988. Requirement of heavy neurofilament subunit in the development of axons with large calibers. *J. Cell Biol.* 143:195–205.

25. Rao, M. V., M. L. Garcia, …, D. W. Cleveland. 2002. Gene replacement in mice reveals that the heavily phosphorylated tail of neurofilament heavy subunit does not affect axonal caliber or the transit of cargoes in slow axonal transport. *J. Cell Biol.* 158:681–693.

26. Garcia, M. L., C. S. Lobsiger, …, D. W. Cleveland. 2003. NF-M is an essential target for the myelin-directed "outside-in" signaling cascade that mediates radial axonal growth. *J. Cell Biol.* 163:1011–1020.

27. Xu, Z., J. R. Marszalek, …, D. W. Cleveland. 1996. Subunit composition of neurofilaments specifies axonal diameter. *J. Cell Biol.* 133: 1061–1069.